Stem Cell Research 55 (2021) 102476

Contents lists available at ScienceDirect

Stem Cell Research

journal homepage: www.elsevier.com/locate/scr

Short report

Human iPSC-derived neural crest stem cells can produce EPO and induce erythropoiesis in anemic mice

Valerio Brizi [a,1], Sara Buttò [a,1], Domenico Cerullo [a], Angelo Michele Lavecchia [a], Raquel Rodrigues-Diez [a], Rubina Novelli [a], Daniela Corna [a], Ariela Benigni [a], Giuseppe Remuzzi [a], Christodoulos Xinaris [a,b,*]

[a] *Istituto di Ricerche Farmacologiche Mario Negri IRCCS, Bergamo, Italy*
[b] *University of Nicosia Medical School, Nicosia, Cyprus*

ARTICLE INFO

Keywords:
Pluripotent stem cells
Neural crest cells
Erythropoietin
Anemia
Erythropoiesis

ABSTRACT

Inadequate production of erythropoietin (EPO) leads to anemia. Although erythropoiesis-stimulating agents can be used to treat anemia, these approaches are limited by high costs, adverse effects, and the need for frequent injections. Developing methods for the generation and transplantation of EPO-producing cells would allow for the design of personalized and complication-free therapeutic solutions. In mice, the first EPO source are neural crest cells (NCCs), which ultimately migrate to the fetal kidney to differentiate into EPO-producing fibroblasts. In humans however, it remains unknown whether NCCs can produce EPO in response to hypoxia. Here, we developed a new protocol to differentiate human induced pluripotent stem cells (hiPSCs) into NCCs and showed that cthese cells can produce functional EPO that can induce human CD34$^+$ hematopoietic progenitor differentiation into erythroblasts *in vitro*. Moreover, we showed that hiPSC-derived NCCs can be embedded in clinical-grade atelocollagen scaffolds and subcutaneously transplanted into anemic mice to produce human EPO, accelerate hematocrit recovery, and induce erythropoiesis in the spleen. Our findings provide unprecedented evidence of the ability of human NCCs to produce functional EPO in response to hypoxia, and proof-of-concept for the potential clinical use of NCC-containing scaffolds as cell therapy for renal and non-renal anemia.

1. Introduction

Erythropoietin (EPO) is a glycoprotein hormone secreted mainly by renal fibroblasts in response to hypoxia to induce erythropoiesis. In patients with chronic kidney disease, EPO production is strongly reduced, leading to renal anemia (Romagnani et al., 2017). Although recombinant human EPO administration minimizes the need for transfusion and associated complications, it is limited by adverse effects, elevated costs and negative effects on patients' quality of life (Casadevall et al., 2002). Attempts to treat renal anemia using genetically modified cells and viral vectors (Brill-Almon et al., 2005), though initially promising, have not yet overcome problems related to safety and long-term adverse effects.

Using an EPO-producing cell type derived from human induced pluripotent stem cells (hiPSCs) could be an ideal therapeutic approach to treating renal anemia, since it would allow for the autologous transplantation and physiological regulation of EPO *in vivo*. In mice, the first source of EPO are neural crest cells (NCCs), which secrete EPO for primitive erythropoiesis in the yolk sac, and ultimately migrate to the kidney (E13.5) to differentiate into EPO-producing fibroblasts (Asada et al., 2011). In humans, however, it remains unknown whether NCCs can also produce EPO and respond physiologically to hypoxia by producing functional EPO. To address these questions, we developed a novel protocol for the differentiation of hiPSCs into NCCs and verified that hiPSCs-derived NCCs can release EPO in response to hypoxia and induce erythropoiesis both *in vitro* and *in vivo*.

---

* Corresponding author at: Istituto di Ricerche Farmacologiche Mario Negri IRCCS, Centro Anna Maria Astori, Science and Technology Park Kilometro Rosso, Department of Molecular Medicine, Via Stezzano, 87, 24126 Bergamo, Italy.

E-mail address: christodoulos.xinaris@marionegri.it (C. Xinaris).

[1] VB and SB have equally contributed to the study.

https://doi.org/10.1016/j.scr.2021.102476
Received 25 January 2021; Received in revised form 11 June 2021; Accepted 21 July 2021
Available online 25 July 2021
1873-5061/© 2021 The Authors. Published by Elsevier B.V. This is an open access article under the CC BY-NC-ND license (http://creativecommons.org/licenses/by-nc-nd/4.0/).

2. Material and methods

2.1. Differentiation of hiPSCs toward EPO-producing NCCs

Human iPSCs (clone IV; RRID:CVCL_IT61) (Benedetti et al., 2018; Imberti et al., 2015) were detached with StemPro Accutase (Cat#A1110501; ThermoFisher), seeded at a concentration of 3 × 10^4 viable cells/cm^2 onto growth-factor-reduced Matrigel (Cat#356231, Corning)-coated plates, cultured in mTeSR1 complete medium for 24 h (Cat#05850, StemCell Technologies) containing 10 µM ROCK-inhibitor (Cat#Y0503, Sigma) and then switched to the differentiation medium: DMEM/F12 + GlutaMAX (Cat#31331, ThermoFisher), 17.5 mg/ml CellMaxx Bovine Albumin (Cat#0219989925, MP Biomedicals^{TM}), 17.5 µg/ml human insulin (Cat#I9278, Sigma), 275 µg/ml human holo-transferrin (Cat#T0665, Sigma), 450 µM 1-thioglycerol (Cat#M6145, Sigma), 0.1 mM non-essential amino acids (Cat#11140050, ThermoFisher)] supplemented with 5 mM lithium chloride (LiCl; L0505, Sigma) for 8 days. Differentiation medium was changed daily. To stimulate EPO production, day 8-differentiated cells were cultured under hypoxic conditions (5% O_2) for 48–72 h. For NCC differentiation via dual SMAD pathway inhibition we used a previously described method (Kreitzer et al., 2013).

2.2. RNA isolation and real time qRT-PCR analysis

Total cellular RNA was extracted and transcribed as previously described (Benedetti et al., 2018). To amplify the cDNA of target genes the ViiA 7 Real Time PCR system (Applied Biosystems), SYBR^{TM} Green PCR Master Mix (Cat#4367659, ThermoFisher) and the primers (3 pmol/µl) listed in Supplementary Table 2 were used. The analysis is described in detail in Supplemental Methods.

2.3. Immunofluorescence analyses in vitro

Cells were fixed with 4% paraformaldehyde (Cat#157-8, Electron Microscopy Sciences), and permeabilized with 0.1% (for EPO staining) or 0.3% TritonX-100 (Cat#93418, Sigma) for 5 min at room temperature (RT). After blocking with BSA, cells were incubated with the primary antibodies overnight at 4 °C. Next, cells were incubated with the appropriate secondary antibodies (Jackson ImmunoResearch Europe) for 1 h at RT. Slides were mounted with Dako Fluorescent Mounting Medium (Cat#S3023, Dako). Digital images were acquired using Apotome Axio Imager Z2 (Carl Zeiss) or an inverted confocal laser scanning microscope (LSM 510 META, Carl Zeiss) and analyzed with ImageJ. For more details see Supplemental Methods.

2.4. Bright-field imaging and monitoring of cellular movement

Bright-field images were obtained using a Primo Vert inverted microscope (Carl Zeiss) and cell migration was monitored by acquiring time-lapse images with the Axio Observer.Z1 cell-observer microscope (Carl Zeiss).

2.5. ELISA assay

Human EPO in the supernatant was measured using a human EPO ELISA kit (Cat#ab119522) following the manufacturer's instructions. The data are from three independent experiments. Total hemoglobin in the spleen's homogenates were measured using a hemoglobin colorimetric kit (Cat#700540, Cayman Chemical) following the manufacturer's instructions.

2.6. Clonogenic hematopoietic progenitor cell assay

The clonogenic assay was applied as previously described (Hitomi et al., 2017). 5 × 10^4 CD34$^+$ HSCs/ml were pre-incubated for 3 h in fresh hiPSC differentiation basal medium (Control) or in EPO-containing supernatant from hiPSC-derived NCCs that were previously submitted to hypoxia for 72 h (EPO group) or in EPO-containing supernatant inactivated by human EPO-neutralizing antibody (Cat#AF959, R&D Systems; 5 µg/ml) (EPO + Inh group), and then transferred to MethoCult™ Enriched (Cat#04435, StemCell Technologies; 1 ml per dish; 5 × 10^3 HSCs/ml) semisolid medium. On days 7 and 11, 100 µl/ml of hiPSC basal medium or supernatant from EPO-producing NCCs were added on top of the semisolid medium in the Control and EPO group, respectively. BFU-E colonies were counted on day 12. For further details see Supplemental Methods.

2.7. Induction of anemia and evaluation of Hct levels

Acute anemia was induced in seven-week-old male NOD/SCID mice (n = 7; Strain code: 394; Charles River) through rapid *retro*-orbital blood withdrawal (20% volemia) on two consecutive days using heparin-coated glass capillary tubes. The Hct baseline levels were measured using a micro-Hct capillary tube reader. To prevent hypovolemia and hypotension, animals were injected intraperitoneally with a volume of saline equal to twice the volume of blood collected immediately after blood withdrawals. The increase in Hct levels in anemic mice was evaluated at different time points after scaffold transplantation by applying the following formula: $(Hct_{dayx}\text{-}Hct_{day2})/Hct_{day2}$, x = 4, 5 and 7). No significant changes to body weight were observed over time.

2.8. Neural Crest Cell-containing scaffold generation and transplantation

Atelocollagen honeycomb disks (Cat#CSH-96, KOKEN Co. Ltd.) were pre-conditioned with warm PBS and centrifuged at 2200×*g* for 3 min in 96-well plate. Next, each disk was submerged with 250 µl of culture medium containing 3.5 × 10^5 hiPSC-derived NCCs on differentiation day 8. After 16 h, culture medium was changed and then after 4 h the scaffolds were transplanted subcutaneously to the dorsal area of anemic mice (n = 4; one scaffold per mouse). Sham-operated mice underwent surgery without scaffold transplantation and served as controls.

2.9. Histological and immunofluorescence analyses of explanted tissues

Five days after transplantation, mice were sacrificed using CO_2 inhalation and grafts and the mice's organs were explanted, embedded in OCT compound (Cat#4583, Tissue-Tek) and frozen. Three-µm sections from grafts or spleens were stained with Harris's hematoxylin or with Mayer's hematoxylin and eosin Y, respectively. For the immunofluorescence staining, 3-µm sections were fixed with 4% PFA for 20 min, blocked/permeabilized using a solution of 10% normal donkey serum (NDS) + 0.3% TritonX-100 for 45 min at RT, and incubated with primary antibodies. Other samples were fixed and permeabilized with ice-cold acetone for 10 min, blocked with 3% BSA for 30 min at RT, and then incubated with mouse anti-human HNK1 diluted in 3% BSA overnight at 4 °C, and FITC-conjugated mouse anti-HNA for 3 h at RT. Next, samples were incubated with the secondary antibodies, stained with DAPI and slides were mounted with Dako. For more details see Supplemental Methods.

2.10. Statistics

Statistical analyses were performed using Graph Pad Prism software (GraphPad). All data are expressed as mean ± SEM. Comparisons were made using Student's *t*-test or one-way ANOVA followed by Tukey's post-hoc test as appropriate. Statistical significance was set at $P < 0.05$.

2.11. Study approval

All procedures involving animals were performed with the approval of and in accordance with the internal institutional guidelines of the

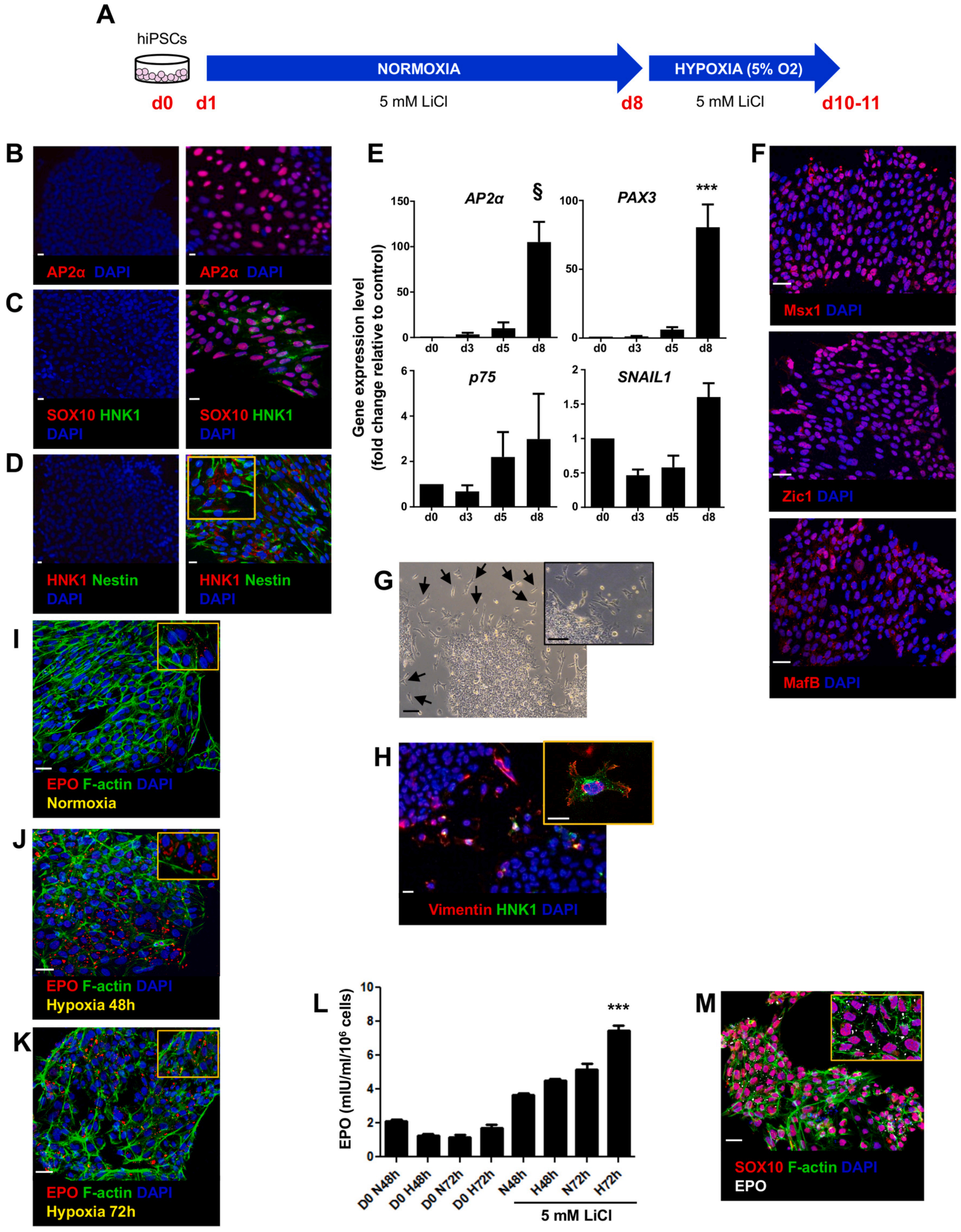
A
hiPSCs
NORMOXIA
HYPOXIA (5% O2)
d0
d1
5 mM LiCl
d8
5 mM LiCl
d10-11
B
AP2α DAPI
AP2α DAPI
C
SOX10 HNK1 DAPI
SOX10 HNK1 DAPI
D
HNK1 Nestin DAPI
HNK1 Nestin DAPI
E
Gene expression level (fold change relative to control)
AP2α
§
150
100
50
0
d0
d3
d5
d8
PAX3
***
100
50
0
d0
d3
d5
d8
p75
6
4
2
0
d0
d3
d5
d8
SNAIL1
2
1.5
1
0.5
0
d0
d3
d5
d8
F
Msx1 DAPI
Zic1 DAPI
MafB DAPI
G
H
Vimentin HNK1 DAPI
I
EPO F-actin DAPI
Normoxia
J
EPO F-actin DAPI
Hypoxia 48h
K
EPO F-actin DAPI
Hypoxia 72h
L
EPO (mIU/ml/10^6 cells)
10
8
6
4
2
0
***
D0 N48h
D0 H48h
D0 N72h
D0 H72h
N48h
H48h
N72h
H72h
5 mM LiCl
M
SOX10 F-actin DAPI
EPO

(caption on next page)

Fig. 1. Human iPSC-derived NCCs produce functional EPO in response to hypoxia. (A) Schematic representation of the protocol for generating hiPSC-derived EPO-producing NCCs. (B–D) Expression of NCC-specific markers in undifferentiated (left panels) and 8-day-differentiated human iPSCs (right panels). Scale bars: 10 μm. (E) Gene expression profile of hiPSCs during differentiation. The mRNA levels of AP2α, PAX3 and p75 peaked on d8. SNAIL1 exhibited slightly reduced expression levels on d3 and d5 that increased again on d8. Values are relative to the housekeeping gene RPL29. $^{\S}P = 0.001$, $^{***}P < 0.001$ versus d0 by one-way ANOVA. (F) Expression of NCC-lineage markers in 8-day-differentiated human iPSCs. Cranial NCC marker Msx1 (top panel, 45.29 ± 3.761% positive cells/total number), trunk NCC marker Zic1 (middle panel, 39.02 ± 4.144% positive cells/total number) and cardiac NCC marker MafB (bottom panel, 9.67 ± 1.473% positive cells/total number). Scale bars: 50 μm. (G, H) Human iPSC-derived NCC motility *in vitro*. (G) Phase-contrast microscopy images displaying many cells with a fibroblast-like morphology (inset) moving out of colonies on d7 (arrows). (H) Migrating cells were positive for HNK1 and the cytoskeletal intermediate filament marker vimentin. Inset: vimentin staining was predominant in lamellipodia of motile cell. Scale bars: 100 μm (F) and 20 μm (G). (I–K) Representative images of EPO production at (I) day 8 of differentiation, and after (J) 48 h and (K) 72 h of hypoxia. (I) At d8, few NCC-differentiated cells exhibited positive staining in their cytoplasm under normoxic conditions. (J, K) Cells that were cultured under hypoxic conditions for (J) 48 h or (K) 72 h and visualized by F-actin labeling, exhibited increased expression of EPO protein in their cytoplasm (inset) (Mean cell number per field in normoxia, 48 h and 72 h hypoxia groups were 239 ± 9.76, 137 ± 14.03 and 110 ± 9.73, respectively). Scale bars: 50 μm. (L) EPO concentration in the supernatant of undifferentiated hiPSCs (d0, control) and hiPSC-derived NCCs grown under normoxic or hypoxic conditions for 48 h and 72 h. Undifferentiated cells secreted negligible levels of EPO under normoxic as well as hypoxic conditions. Differentiated NCCs produced significantly higher amounts of EPO after 72 h of hypoxia (7.447 ± 0.312 mlU/ml/10^6 cells) compared to all other tested conditions (N48h: 3.641 ± 0.131, H48h: 4.509 ± 0.114, and N72h: 5.171 ± 0.341 mlU/ml/10^6 cells). $^{***}P < 0.001$ vs all culture conditions tested by one-way ANOVA. N, normoxia; H, hypoxia; h, hours. (M) Neural crest cells cultured under hypoxic condition for 72 h expressing SOX10 in the nucleus and releasing EPO (mean of EPO-producing cells on total cells: 28.51 ± 1.413%). Scale bars: 50 μm.

Istituto di Ricerche Farmacologiche Mario Negri IRCCS, which are in compliance with national (D.L.n.26, March 4, 2014) and international laws and policies (directive 2010/63/EU on the protection of animals used for scientific purposes).

3. Results

3.1. Differentiation of hiPSCs into NCCs

Wnt signaling is required for neural crest specification, and GSK3β inhibition – followed by the consequent β–catenin activation – are crucial steps in the activation of the canonical Wnt pathway (Elkouby and Frank, 2010; Ji et al., 2019). To induce NCC differentiation we treated hiPSCs with lithium chloride (LiCl) (Fig. 1A) – a strong inhibitor of GSK3β (Jamieson et al., 2011; Stambolic et al., 1996). LiCl robustly induced β–catenin expression, nuclear localization/translocation (Supplementary Fig. 1), and ectoderm lineage and subsequent NC differentiation, as identified based on the timely expression of specific markers (Supplementary Fig. 2, Fig. 1). At day 8, all the differentiated cells were positive for SOX10, and most cells highly expressed AP2α, HNK1 (Betters et al., 2010) and Nestin (Lothian and Lendahl, 1997) (Fig. 1B–D). The gene expression profile analysis showed that AP2α, PAX3 (Wu et al., 2008) and p75 (Huang et al., 2016) mRNA levels increased markedly over time, reaching peak expression on d8 (105.1 ± 22.2-fold vs d0, 80.5 ± 16.6-fold vs d0, and 3.0 ± 2.0-fold vs d0, respectively) (Fig. 1E). The expression of SNAIL1 (Minamino et al., 2015) decreased slightly on d3 and d5 (0.5 ± 0.08- and 0.6 ± 0.2-fold vs d0, respectively) and increased again on d8 (1.6 ± 0.2-fold vs d0) (Fig. 1E). Further immunofluorescence analyses have shown that the dominant crest populations were of cranial (Ishii et al., 2005) and trunk (Simões-Costa et al., 2012) lineages, and to a small proportion were cardiac NCCs (Tani-Matsuhana et al., 2018) (Fig. 1F), in analogy to earlier studies showing that Wnt activation predominantly gives rise to cranial and trunk NCCs (Ji et al., 2019).

NCCs have remarkable motility (Bronner-Fraser, 1993). The onset of NCC migration requires changes in cytoskeletal organization and composition, such as the replacement of keratin filaments with vimentin intermediate filaments and the migration of peripheral cells (in a process known as delamination) to the various tissues (Klymkowsky, 2019). Live cell analysis showed individual cells migrating from the peripheral area of the colonies between d6 and d7 (Fig. 1G; Supplementary Movie 1). These cells changed morphology (Fig. 1G) and expressed vimentin in lamellipodial regions (Helfand et al., 2011) (Fig. 1H), and overexpressed nuclear SOX10, as do *in vivo* migrating NCCs (McKeown et al., 2005) (Supplementary Fig. 3A). These results demonstrated that our protocol efficiently induces hiPSCs to differentiate into NCCs that express a spectrum of NC markers and form classic colonies with peripheral migrating NCCs.

3.2. Human iPSC-derived NCCs respond to hypoxia by releasing EPO

Next, we analyzed the capacity of NCCs to produce and secrete EPO under normoxic and hypoxic (5% O_2) conditions *in vitro*. Compared to normoxia (Fig. 1I), hypoxia increased EPO production in the cytoplasm of NCC (Fig. 1J, K; Supplementary Fig. 3B), which was gradually released into the medium to reach significantly increased levels by 72 h (Fig. 1L). At this time point almost 30% of NCCs produced EPO (Fig. 1M). To examine whether the production of EPO was an intrinsic effect of our protocol or a ubiquitous capacity of human NCCs, we differentiated NCCs using a protocol based on the modulation of another pathway (Kreitzer et al., 2013). Remarkably, NCCs that were generated through the inhibition of the SMAD pathway were also able to produce EPO in response to hypoxia (Supplementary Fig. 4). Our data demonstrate that hiPSC-derived NCCs can produce and release EPO and are highly responsive to hypoxia. Moreover, they also suggest that NCCs secrete EPO for primitive erythropoiesis not only in mouse but also in human embryos.

3.3. Neural Crest Cell-released EPO induces human erythropoiesis in vitro

One of the key functions of NCCs in the early mouse embryo is the secretion of EPO, which is essential for erythropoiesis in the yolk sac and for sufficient oxygen supply in the whole embryo *in utero* (Hirano and Suzuki, 2019).

To test whether the NCC-derived EPO had erythropoietic activity, we exposed human $CD34^+$ Haemopoietic Stem Cells to the supernatant of NCCs that were previously cultured under hypoxic conditions for 72 h (EPO group) (Fig. 2A-C) and quantified the clonal burst-forming unit erythroid (BFU-E) colonies (Hitomi et al., 2017; Xi et al., 2013). Treated cells formed significantly more BFU-E colonies (Fig. 2C, D) than the control group (Fig. 2B, D), and also exhibited more intense red pigmentation, indicating hemoglobin production (Fig. 2C). This response was abolished when supernatant was treated with an EPO-neutralizing antibody (Chen et al., 2018) (Supplementary Fig. 5). These results suggest that, in response to hypoxia, NCCs release functional EPO that can stimulate human erythropoiesis.

3.4. EPO-producing NCCs accelerate hematocrit recovery in vivo and induce splenic erythropoiesis

To evaluate whether our hiPSC-derived NCCs could respond to hypoxia *in vivo* and improve anemia recovery, we incorporated NCCs

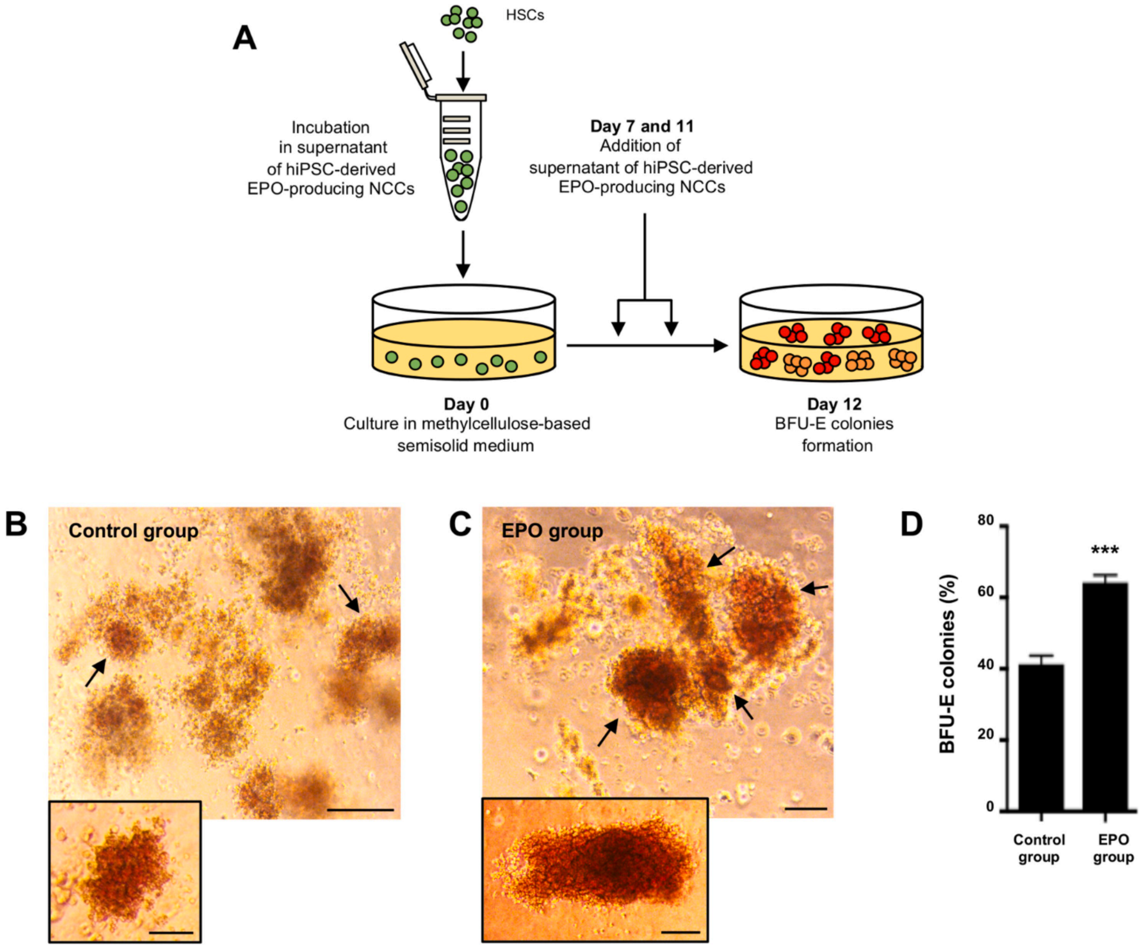

Fig. 2. EPO produced by NCC-differentiated cells stimulates HSC differentiation in BFU-E colonies. (A) Schematic representation of the colony-forming unit assay for evaluating the capacity of EPO produced by NCCs to induce HSC differentiation into erythroblasts (BFU-E colonies). (B, C) Colonies formed in the clonogenic hematopoietic progenitor cell assay at day 12 in (B) control and (C) EPO groups. BFU-E colonies (arrows) in the EPO group were more numerous and larger (insets) than in the control group and easily distinguishable from other HSC-derived colonies due to the erythroblasts' characteristic reddish color. Scale bars: 100 μm. (D) Percentage of BFU-E colonies formed in control (41.31 ± 2.372%) and EPO (64.27 ± 2.009%) groups in the total number of colonies. $^{***}P < 0.001$ by Student's *t*-test. Data shown are expressed as mean ± SEM.

into atelocollagen disks (Ishikawa et al., 2017) (Fig. 3A-C), and transplanted them subcutaneously into anemic NOD/SCID mice (Fig. 3D). Anemia was induced by adapting our previous rat model of acute anemia (Xinaris et al., 2012) to mice through rapid blood withdrawals on days 0 and 1. On day 2, when the hematocrit (Hct) levels had decreased significantly (Supplementary Table 1) we transplanted the NCC-containing scaffolds (Fig. 3D; Supplementary Fig. 6) and then sacrificed the mice 5 days after transplantation. Analysis of explanted grafts (Fig. 3E) showed that large numbers of cells had remained attached to the inside of the scaffolds (Fig. 3F), were still positive for the NCC-specific markers SOX10 and HNK1 (Fig. 3G,H), and produced EPO (Fig. 3I); on the other hand, few cells showed signs of apoptosis (Supplementary Fig. 7), suggesting that embedded cells did not suffer any significant stress under the skin. Remarkably, when we measured Hct in transplanted and control mice 2 (d4), 3 (d5) and 5 (d7) days after transplantation (Fig. 3A and Supplementary Table 1), we found that the NCC-containing scaffolds significantly accelerated the rise in Hct levels 3 days (d5) after transplantation (Fig. 3J). Further analysis of the spleen – which plays an important role in murine extramedullary erythropoiesis after bleeding (Paulson et al., 2011) – showed a strikingly greater expansion of the red pulp in transplanted animals (arrows Fig. 3K), and a two-fold increase in splenic hemoglobin (Fig. 3L) compared to untransplanted controls.

These results demonstrate that hiPSC-derived NCCs survive in atelocollagen scaffolds, can physiologically respond to anemia, and efficiently induce erythropoiesis *in vivo*. In terms of developing cell therapy for renal anemia in the future, this system exhibits important potential for translation, since the atelocollagen has already been used clinically in a variety of applications (Tohyama et al., 2009), and subcutaneous implantation meets the requirement for easy clinical application. Nevertheless, future studies should focus on evaluating safety and therapeutic efficacy in a chronic anemia model, the long-term survival of engineered tissues, and the overall optimization of the system based on blood parameters to generate the best long-term therapeutic outcomes.

4. Conclusions

Here we developed a simple and robust protocol for the differentiation of hiPSCs into NCCs and showed the hitherto unknown ability of human NCCs to efficiently respond to hypoxia and produce functional EPO. Moreover, we showed that NCC implants accelerate the normalization of hematocrit and strongly induce splenic erythropoiesis after anemia, confirming the capacity of these cells to efficiently induce erythropoiesis *in vivo*. Despite the existing limitations of the study (e.g. the need for safety and efficacy evaluation in long-term

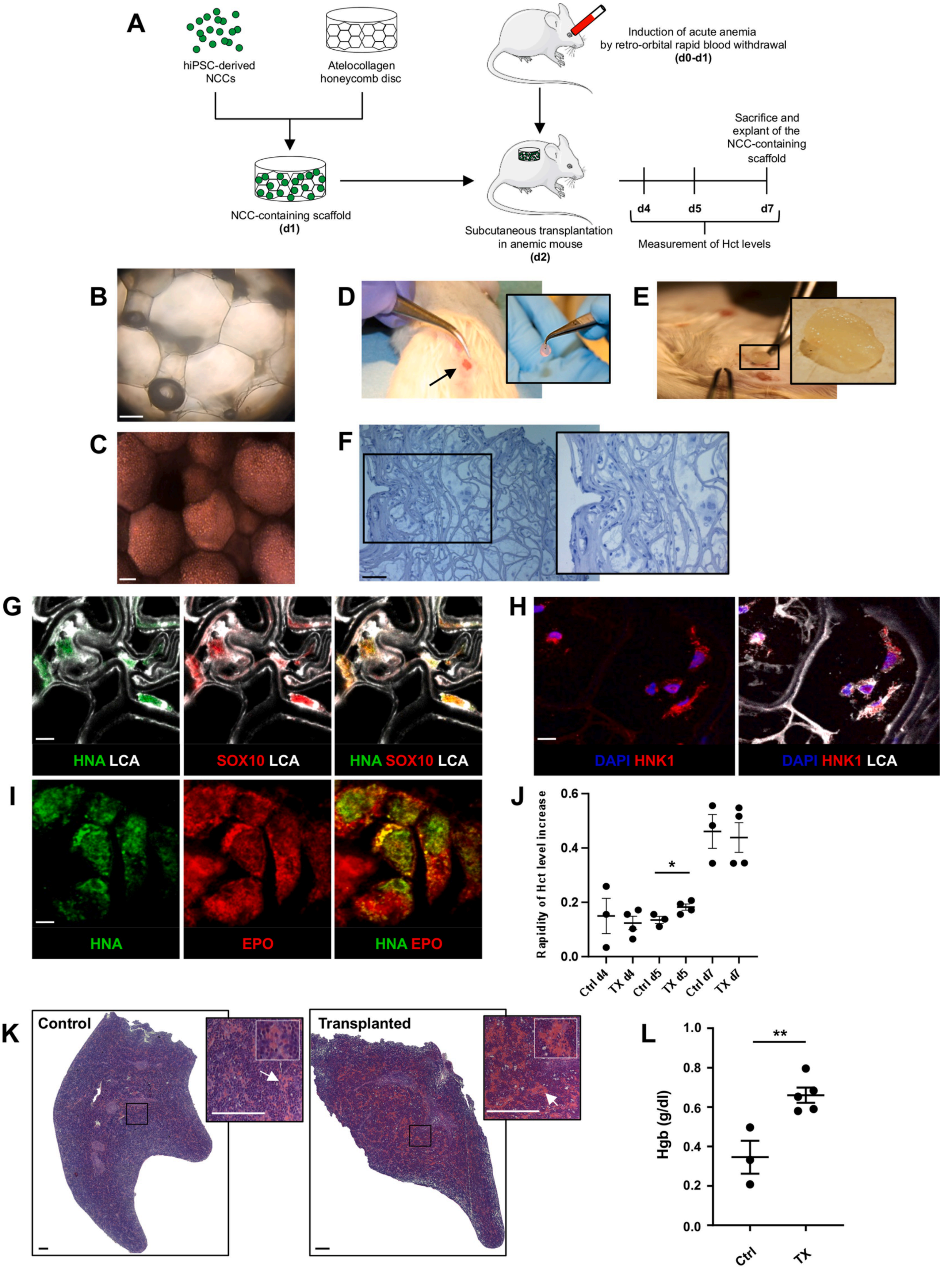
A
hiPSC-derived NCCs
Atelocollagen honeycomb disc
NCC-containing scaffold (d1)
Induction of acute anemia by retro-orbital rapid blood withdrawal (d0-d1)
Subcutaneous transplantation in anemic mouse (d2)
Sacrifice and explant of the NCC-containing scaffold
d4
d5
d7
Measurement of Hct levels
B
C
D
E
F
G
HNA LCA
SOX10 LCA
HNA SOX10 LCA
H
DAPI HNK1
DAPI HNK1 LCA
I
HNA
EPO
HNA EPO
J
Rapidity of Hct level increase
0.0
0.2
0.4
0.6
*
Ctrl d4
TX d4
Ctrl d5
TX d5
Ctrl d7
TX d7
K
Control
Transplanted
L
Hgb (g/dl)
0.0
0.2
0.4
0.6
0.8
1.0
**
Ctrl
TX

(caption on next page)

Fig. 3. NCC-differentiated cells respond to hypoxia and accelerate anemia recovery *in vivo*. (A) Schematic representation of *in vivo* experiment. (B, C) Phase-contrast microscopy images of empty (A) and NCC-containing (B) atelocollagen honeycomb disks before implantation. Scale bars: 100 μm. (D) A NCC-containing scaffold (inset) was transplanted into a dorsal subcutaneous pocket (arrow) created by making an incision in the dorsal aspect of an anemic mouse. (E) A NCC-containing scaffold that was explanted from mice sacrificed 5 days after transplantation. The explanted scaffold maintained structural integrity (inset). (F) Hematoxylin-stained section of an explanted graft. Several cells were visible within the scaffold and adhered to the atelocollagen fibers (inset). Scale bar: 200 μm. (G–I) The human cells that were found attached to the fibers (white) of explanted scaffolds still expressed (G) SOX10 (red) in their nuclei and (H) HNK1 (red) in their cytoplasm, and (I) highly expressed EPO. HNA, human nuclear antigen. Scale bars: 5 μm. (J) Hct levels in control (Ctrl) and transplanted (TX) anemic mice over time. The rise in Hct levels was significantly faster in TX mice 3 days (d5) after transplantation than in control mice. The acceleration of the increase in Hct levels was calculated by applying the formula described in Section 2.7. $^*P < 0.05$ by Student's *t*-test. (K) Representative images of hematoxylin and eosin-stained spleen sections of control (left) and transplanted (right) anemic mice. A greater induction of erythropoiesis shown by a massive expansion of red pulp occurs in the spleen of transplanted mice (arrows in the inset). Scale bars: 250 μm (L) Hemoglobin (Hgb) concentration in spleen lysate of control and transplanted (TX) anemic mice. The transplantation of NCC-containing scaffolds results in a significant increase of Hgb levels. ** $P < 0.01$ by Student's *t*-test. (For interpretation of the references to color in this figure legend, the reader is referred to the web version of this article.)

conditions), both this novel methodology and the knowledge that human NCCs can produce functional EPO, may provide a technical and conceptual basis for the development of a novel cell therapy for renal and non-renal anemia.

CRediT authorship contribution statement

Valerio Brizi: Conceptualization, Methodology, Writing - original draft, Data curation, Formal analysis, Investigation, Validation, Visualization. **Sara Buttò:** Validation, Investigation, Methodology, Formal analysis, Data curation, Visualization. **Domenico Cerullo:** Investigation, Validation, Methodology. **Angelo Michele Lavecchia:** Methodology, Review & editing. **Raquel Rodrigues-Diez:** Conceptualization, Methodology, Investigation. **Rubina Novelli:** Writing - review & editing. **Daniela Corna:** Investigation, Validation. **Ariela Benigni:** Review & editing. **Giuseppe Remuzzi:** Review & editing. **Christodoulos Xinaris:** Conceptualization, Supervision, Writing - original draft, Project administration, Funding acquisition.

Declaration of Competing Interest

The authors declare that they have no known competing financial interests or personal relationships that could have appeared to influence the work reported in this paper.

Acknowledgments

The authors wish to thank Lorena Longaretti, Susanna Tomasoni and Francesca Vitari for technical advice, and Kerstin Mierke for excellent editing work on the manuscript. We would like also thank Mary Louise Wratten (Bellco/Medtronic) for helping us to initiate and develop this project. VB, AML and RN were recipients of fellowships from Fondazione Aiuti per la Ricerca sulle Malattie Rare, Bergamo, Italy. RRD was a recipient of the ERA-EDTA Longterm fellowship (LTF 128-2012). This research was funded by Medtronic Inc. The authors gratefully thank Associazione per la Ricerca sul Diabete Italia (ARDI) for continued support.

Appendix A. Supplementary data

Supplementary data to this article can be found online at https://doi.org/10.1016/j.scr.2021.102476.

References

Asada, N., Takase, M., Nakamura, J., Oguchi, A., Asada, M., Suzuki, N., Yamamura, K.-I., Nagoshi, N., Shibata, S., Rao, T.N., Fehling, H.J., Fukatsu, A., Minegishi, N., Kita, T., Kimura, T., Okano, H., Yamamoto, M., Yanagita, M., 2011. Dysfunction of fibroblasts of extrarenal origin underlies renal fibrosis and renal anemia in mice. J. Clin. Invest. 121 (10), 3981–3990. https://doi.org/10.1172/JCI5730110.1172/JCI57301DS1.

Benedetti, V., Brizi, V., Guida, P., Tomasoni, S., Ciampi, O., Angeli, E., Valbusa, U., Benigni, A., Remuzzi, G., Xinaris, C., 2018. Engineered kidney tubules for modeling patient-specific diseases and drug discovery. EBioMedicine 33, 253–268. https://doi.org/10.1016/j.ebiom.2018.06.005.

Betters, E., Liu, Y., Kjaeldgaard, A., Sundström, E., García-Castro, M.I., 2010. Analysis of early human neural crest development. Dev. Biol. 344 (2), 578–592. https://doi.org/10.1016/j.ydbio.2010.05.012.

Brill-Almon, E., Stern, B., Afik, D., Kaye, J., Langer, N., Bellomo, S., Shavit, M., Pearlman, A., Lippin, Y., Panet, A., Shani, N., 2005. Ex vivo transduction of human dermal tissue structures for autologous implantation production and delivery of therapeutic proteins. Mol. Ther. J. Am. Soc. Gene Ther. 12 (2), 274–282. https://doi.org/10.1016/j.ymthe.2005.03.023.

Bronner-Fraser, M., 1993. Mechanisms of neural crest cell migration. BioEssays News Rev. Mol. Cell. Dev. Biol. 15 (4), 221–230. https://doi.org/10.1002/(ISSN)1521-187810.1002/bies.v15:410.1002/bies.950150402.

Casadevall, N., Nataf, J., Viron, B., Kolta, A., Kiladjian, J.-J., Martin-Dupont, P., Michaud, P., Papo, T., Ugo, V., Teyssandier, I., Varet, B., Mayeux, P., 2002. Pure red-cell aplasia and antierythropoietin antibodies in patients treated with recombinant erythropoietin. N. Engl. J. Med. 346 (7), 469–475. https://doi.org/10.1056/NEJMoa011931.

Chen, Y.-H., Feng, H.-L., Jeng, S.-S., 2018. Zinc supplementation stimulates red blood cell formation in rats. Int. J. Mol. Sci. 19 (9), 2824. https://doi.org/10.3390/ijms19092824.

Elkouby, Y.M., Frank, D., 2010. Neural crest induction. Morg. Claypool Life Sci.

Helfand, B.T., Mendez, M.G., Murthy, S.N.P., Shumaker, D.K., Grin, B., Mahammad, S., Aebi, U., Wedig, T., Wu, Y.I., Hahn, K.M., Inagaki, M., Herrmann, H., Goldman, R.D., Omary, M.B., 2011. Vimentin organization modulates the formation of lamellipodia. Mol. Biol. Cell 22 (8), 1274–1289. https://doi.org/10.1091/mbc.e10-08-0699.

Hirano, I., Suzuki, N., 2019. The neural crest as the first production site of the erythroid growth factor erythropoietin. Front. Cell Dev. Biol. 7 https://doi.org/10.3389/fcell.2019.00105.

Hitomi, H., Kasahara, T., Katagiri, N., Hoshina, A., Mae, S.-I., Kotaka, M., Toyohara, T., Rahman, A., Nakano, D., Niwa, A., Saito, M.K., Nakahata, T., Nishiyama, A., Osafune, K., 2017. Human pluripotent stem cell–derived erythropoietin-producing cells ameliorate renal anemia in mice. Sci. Transl. Med. 9 (409), eaaj2300. https://doi.org/10.1126/scitranslmed.aaj2300.

Huang, M., Miller, M.L., McHenry, L.K., Zheng, T., Zhen, Q., Ilkhanizadeh, S., Conklin, B. R., Bronner, M.E., Weiss, W.A., 2016. Generating trunk neural crest from human pluripotent stem cells. Sci. Rep. 6, 19727. https://doi.org/10.1038/srep19727.

Imberti, B., Tomasoni, S., Ciampi, O., Pezzotta, A., Derosas, M., Xinaris, C., Rizzo, P., Papadimou, E., Novelli, R., Benigni, A., Remuzzi, G., Morigi, M., 2015. Renal progenitors derived from human iPSCs engraft and restore function in a mouse model of acute kidney injury. Sci. Rep. 5, 8826. https://doi.org/10.1038/srep08826.

Ishii, M., Han, J., Yen, H.-Y., Sucov, H.M., Chai, Y., Maxson, R.E., 2005. Combined deficiencies of Msx1 and Msx2 cause impaired patterning and survival of the cranial neural crest. Dev. Camb. Engl. 132, 4937–4950. https://doi.org/10.1242/dev.02072.

Ishikawa, M., Ohnishi, H., Skerleva, D., Sakamoto, T., Yamamoto, N., Hotta, A., Ito, J., Nakagawa, T., 2017. Transplantation of neurons derived from human iPS cells cultured on collagen matrix into guinea-pig cochleae. J. Tissue Eng. Regen. Med. 11 (6), 1766–1778. https://doi.org/10.1002/term.v11.610.1002/term.2072.

Jamieson, C., Sharma, M., Henderson, B.R., 2011. Regulation of β-catenin nuclear dynamics by GSK-3β involves a LEF-1 positive feedback loop. Traffic 12, 983–999. https://doi.org/10.1111/j.1600-0854.2011.01207.x.

Ji, Y.u., Hao, H., Reynolds, K., McMahon, M., Zhou, C.J., 2019. Wnt signaling in neural crest ontogenesis and oncogenesis. Cells 8 (10), 1173. https://doi.org/10.3390/cells8101173.

Klymkowsky, M.W., 2019. Filaments and phenotypes: cellular roles and orphan effects associated with mutations in cytoplasmic intermediate filament proteins. F1000Research 8. 10.12688/f1000research.19950.1.

Kreitzer, F.R., Salomonis, N., Sheehan, A., Huang, M., Park, J.S., Spindler, M.J., Lizarraga, P., Weiss, W.A., So, P.L., Conklin, B.R., 2013. A robust method to derive functional neural crest cells from human pluripotent stem cells. Am J Stem Cells 2, 119–131.

Lothian, C., Lendahl, U., 1997. An evolutionarily conserved region in the second intron of the human nestin gene directs gene expression to CNS progenitor cells and to early neural crest cells. Eur. J. Neurosci. 9, 452–462.

McKeown, S.J., Lee, V.M., Bronner-Fraser, M., Newgreen, D.F., Farlie, P.G., 2005. Sox10 overexpression induces neural crest-like cells from all dorsoventral levels of the neural tube but inhibits differentiation. Dev. Dyn. Off. Publ. Am. Assoc. Anat. 233 (2), 430–444. https://doi.org/10.1002/dvdy.20341.

Minamino, Y., Ohnishi, Y., Kakudo, K., Nozaki, M., 2015. Isolation and propagation of neural crest stem cells from mouse embryonic stem cells via cranial neurospheres. Stem Cells Dev. 24 (2), 172–181. https://doi.org/10.1089/scd.2014.0152.

Paulson, R.F., Shi, L., Wu, D.-C., 2011. Stress erythropoiesis: new signals and new stress progenitor cells. Curr. Opin. Hematol. 18 (3), 139–145. https://doi.org/10.1097/MOH.0b013e32834521c8.

Romagnani, P., Remuzzi, G., Glassock, R., Levin, A., Jager, K.J., Tonelli, M., Massy, Z., Wanner, C., Anders, H.-J., 2017. Chronic kidney disease. Nat. Rev. Dis. Primer 3, 17088. https://doi.org/10.1038/nrdp.2017.88.

Simões-Costa, M.S., McKeown, S.J., Tan-Cabugao, J., Sauka-Spengler, T., Bronner, M.E., Kondoh, H., 2012. Dynamic and differential regulation of stem cell factor FoxD3 in the neural crest is Encrypted in the genome. PLoS Genet. 8 (12), e1003142. https://doi.org/10.1371/journal.pgen.1003142.

Stambolic, V., Ruel, L., Woodgett, J.R., 1996. Lithium inhibits glycogen synthase kinase-3 activity and mimics wingless signalling in intact cells. Curr. Biol. CB 6 (12), 1664–1669. https://doi.org/10.1016/S0960-9822(02)70790-2.

Tani-Matsuhana, S., Vieceli, F.M., Gandhi, S., Inoue, K., Bronner, M.E., 2018. Transcriptome profiling of the cardiac neural crest reveals a critical role for MafB. Dev. Biol. 444 (Suppl 1), S209–S218. https://doi.org/10.1016/j.ydbio.2018.09.015.

Tohyama, H., Yasuda, K., Minami, A., Majima, T., Iwasaki, N., Muneta, T., Sekiya, I., Yagishita, K., Takahashi, S., Kurokouchi, K., Uchio, Y., Iwasa, J., Deie, M., Adachi, N., Sugawara, K., Ochi, M., 2009. Atelocollagen-associated autologous chondrocyte implantation for the repair of chondral defects of the knee: a prospective multicenter clinical trial in Japan. J. Orthop. Sci. Off. J. Jpn. Orthop. Assoc. 14 (5), 579–588. https://doi.org/10.1007/s00776-009-1384-1.

Wu, M., Li, J., Engleka, K.A., Zhou, B., Lu, M.M., Plotkin, J.B., Epstein, J.A., 2008. Persistent expression of Pax3 in the neural crest causes cleft palate and defective osteogenesis in mice. J. Clin. Invest. 118, 2076–2087. https://doi.org/10.1172/JCI33715.

Xi, J., Li, Y., Wang, R., Wang, Y., Nan, X., He, L., Zhang, P., Chen, L., Yue, W., Pei, X., 2013. In Vitro Large Scale Production of Human Mature Red Blood Cells from Hematopoietic Stem Cells by Coculturing with Human Fetal Liver Stromal Cells [WWW Document]. BioMed Res. Int. 10.1155/2013/807863.

Xinaris, C., Benedetti, V., Rizzo, P., Abbate, M., Corna, D., Azzollini, N., Conti, S., Unbekandt, M., Davies, J.A., Morigi, M., Benigni, A., Remuzzi, G., 2012. In vivo maturation of functional renal organoids formed from embryonic cell suspensions. J. Am. Soc. Nephrol. JASN 23 (11), 1857–1868. https://doi.org/10.1681/ASN.2012050505.